

Super Resolution Imaging of Material Properties Using MEMS Near-Field Microwave Spatial Modulator Arrays

Run Wang, *Student Member, IEEE*, and Massood Tabib-Azar, *Senior Member, IEEE*

Department of Electrical Engineering and Computer Science, Case Western Reserve University, Cleveland, OH, USA

Abstract—Near-field microwave probes were developed and used to image electromagnetic properties of materials with spatial resolutions only limited by the probe aperture size, signal-to-noise ratio and not by the Abbé barrier. The price of this “super” resolution is point-by-point scanning of the sample that makes it slow and requires additional mechanisms to control the probe-to-sample distance during the scan. Here we discuss a new technique that combines aspects of the “free-space” imaging with the super resolution of near-field scanning probes by using an array of local scatterers near the sample. Upon illumination with microwaves, the array of local scatterers generates near-fields near the sample. The near-fields interact with the nearby sample and modulate the reflection coefficient of the scatterers in the array. Vibrating or rotating different scatterers at different base frequency, the reflected microwaves are multiplexed by the array and then de-multiplexed at the receiver to reveal the 2-D spatial field. We implemented applications of this technique in imaging a non-homogenous dielectric sample at 10 GHz using an array of micromotors as scatterers. We also imaged carbon nanotubes using an atomic force microscope tip as the local scatterer with an unprecedented resolution of 5nm at 100GHz.

Keywords- *local scatterer; microwave imaging; near-field microwave; spatial modulator;*

I. INTRODUCTION

Scanning local probe microscopy techniques have advanced our knowledge of surfaces and materials at atomic scales. Local probe microscopy that includes tools such as scanning tunneling microscope (STM) [1], scanning near-field optical microscopy (SNOM) [2], atomic force microscopes (AFM) [3], magnetic force microscope (MFM) [4], and magnetic resonance force microscopy (MRFM) [5] has revealed detailed information regarding atoms at and near material surfaces, mechanical properties at nanometer scale and local columbic and spin interactions.

The scanning near-field microwave microscope (SNM) also belongs to the family of local probes with the ability to “see” inside the sample using electromagnetic waves over a wide range of frequencies [6-12]. For example, the nucleus inside a breast cancerous cell was imaged in-vitro without harming the cell using a ~1-3 GHz near-field microwave probe integrated with AFM [13]. The scanning near-field microscope can be very valuable in performing surface and subsurface imaging of embedded nanostructures, leading to an in-depth understanding of interactions between microscopic objects and their environments. Moreover, the scanning near-

field microscope has the unique ability to provide direct images of subsurface structures owing to the penetration and possible resonant absorption of its electromagnetic signal inside materials.

Our group has integrated the near-field microwave probe on an atomic force microscope probe to simultaneously perform AFM topography and microwave imaging at nanometer scale [14-16]. The results are quite interesting since AFM enables identifying objects by essentially following their contour the way we may identify objects in a dark room where we cannot see the objects by simply touching them. By using microwave near the AFM tip, it is like using the light “seeing” or “sensing” the objects inside the room. The added benefit of the integrated AFM-microwave scanning system is that one can obtain simultaneous AFM and scanning near-field microwave images, and take advantage of the familiar AFM and its knowledge base to validate and reference microwave images for better “registration” of various features.

However, the microwave waveguides that are integrated with the AFM probe are usually lossy and quite dispersive, limiting the ability of the SNM to image over wide frequency range and leading to complications in quantitative measurements. Thus, to enable the AFM probe to perform SNM over a wide frequency range, it is necessary to develop a different method to generate and measure near-fields at the AFM tip. Here we discuss a technique that uses a local scatterer such as a conducting AFM tip or an array of local scatterers such as micromotors to facilitate near-field microwave imaging using traveling waves [17].

In the AFM case, the microwave passing through the sample is reflected back by the conducting AFM tip (the tip may be vibrated in the non-contact mode), which is kept near the sample at a constant distance. Provided that the AFM probe is conducting and that the sample is at least partially transmitting, the reflected microwave will be affected by the interaction between the AFM tip and the sample. In this method, the conducting AFM tip acts as a small antenna that receives and reflects the microwave as schematically shown in fig. 1. The coupling between the AFM tip and the sample determines the reflected wave. Provided that the distance between the tip and the sample is kept constant, the coupling between the tip and the sample is primarily affected by the electromagnetic properties of the sample. Thus, the main contributor to the reflected signal is the electromagnetic property of the sample under test. Parallel AFM probe tips,

vibrated at different frequencies can be used to acquire the near-field image over large surface areas [18].

The “local scatterer” approach will work best in the transmission mode for dielectrics and resistive samples. The technique should be operated in the reflection mode in metals where the transmission will suffer large attenuations.

Measuring and monitoring the local dielectric property may be used to detect voids, porosity and delamination in composite materials [19]. Moreover, once the dielectric properties of a material are known, it is possible to detect its thickness variations [20]. Dielectric properties of mostly in-vitro (excised) biological tissues at radio and microwave frequencies have been the subject of research for over four decades [23-24]. This study covers a large selection of healthy tissues over a wide spectrum of frequencies (10 GHz- 20 GHz). A few studies have also been conducted on the dielectric properties of cancers in a variety of tissue types at radio and microwave frequencies [25]. Typical differences in the permittivity between the normal and malignant tissues are 10-20%. The technique discussed here also lends itself to detection and in-vivo imaging of tumors and other biological objects that have become of great interest recently [26-29].

Before implementing with the AFM system, we devised a larger scale setup using micromotors. A 4x4 array of micromotors were used. Fast data collection and imaging were achieved by exciting different micromotors (local scatterers) at different radial frequencies and using a set of band-pass filters to separate different frequency components. This multiplexing/demultiplexing approach enabled using a single microwave horn antenna to collect spatial information from different micromotors in the array. The array design, a simple theory to quantify the images, and the calibration procedure using multiple measurement points corresponding to different dielectric permittivities were also implemented as discussed next.

II. PRINCIPLE OF OPERATION

Fig. 1 shows a simplified wave reflection and transmission schematic for the scattering problem. As can be seen, the near field waves are generated at the backside of the sample and at the surface of the scatterers. Linearly polarized microwaves are transmitted by a horn antenna and propagate through the sample under investigation as schematically shown in fig. 2. The electromagnetic wave is reflected and partially transmitted at the incident plane of the dielectric sample. The transmitted partial waves finally reach the backside of the sample where an array of local scatterers is located. The electromagnetic wave interacts with the metallic sections of the local scatterers generating current densities on them. The local scatterers are located very near the sample. Thus, their current densities induce charges and secondary current densities in the sample. The interaction between the local scatterers and the sample is capacitively determined by the distance between them. It passes through the sample again and is picked up by the same horn antenna. The reflected signal will be detected by the three-port circulator. The modulation frequency is almost same as the motor frequency, which can be easily recognized at the receiver. Ideally, a

motor array with each motor working at different frequency modulates and reflects the microwave passing through the sample. The signals from different sections of the sample can be detected and recognized accordingly by using a bank of bandpass filters tuned to only pass the signal from one scatterer in the array.

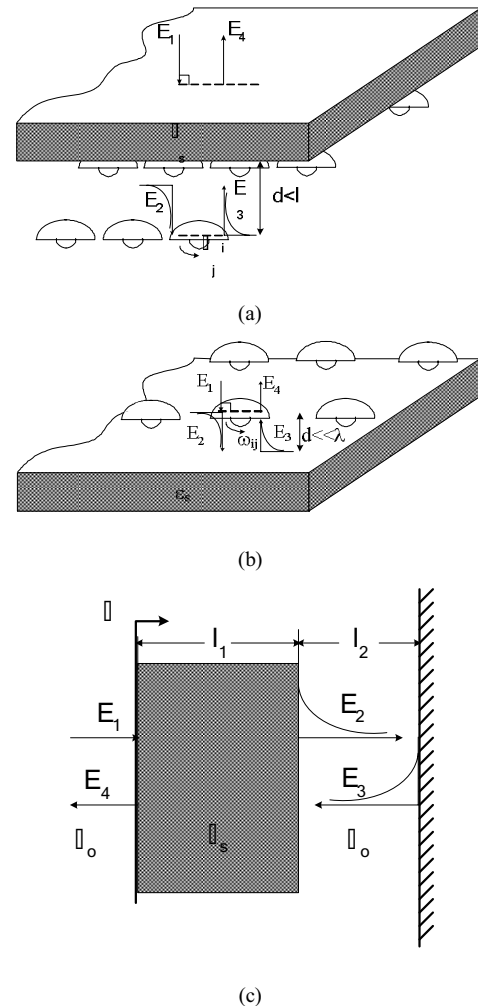


Figure 1. Filed across the interface of dielectric sample,(a) transmission mode, (b) reflection mode, and (c) cross section diagram of dielectric and motor.

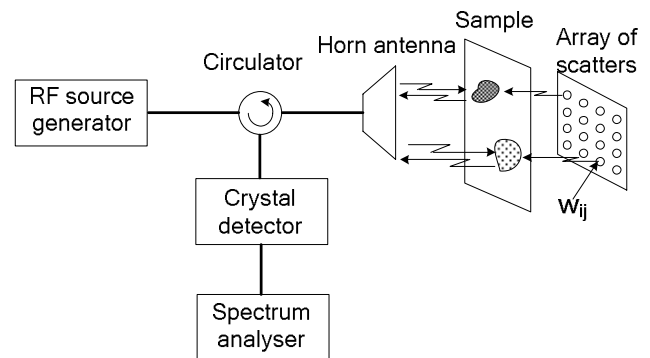


Figure 2. Experimental setup.

The spatial resolution of the final image depends upon both on the size of the local scatterer, its distance from the sample, and on the distance between the horn antenna and the sample. The problem of reconstruction of distribution of the dielectric permittivity ϵ of an object was considered under the following assumptions: 1) propagation of electromagnetic radiation is considered in two-dimensional scalar case under a plane wave illumination and 2) the object scatters radiation on small angles. In this case the initial problem reduces into a simplified wave reflection and transmission problem, as shown in fig. 1(c). A linearly polarized uniform plane wave is assumed normally incident on the dielectric. l_1 is the thickness of the dielectric and l_2 is the distance from the dielectric and the local scatterer surface which is facing the horn antenna. Z_s is the characteristic impedance for the dielectric which is defined as: $Z_s = Z_0 / \sqrt{\epsilon_s}$, where Z_0 is the characteristic impedance for free-space given by $Z_0 = \sqrt{\mu_0 / \epsilon_0} \approx 377 \Omega$. Complex phase constant for the dielectric and free-space is defined as: $\beta_s = 2\pi\sqrt{\epsilon_s} / \lambda_0$ and $\beta_0 = 2\pi / \lambda_0$. Therefore, by using the transmission line theory, it can be shown that the input impedance Z_1 for the dielectric and the motor plane is given by $Z_1 = j(X_0 Z_0 + X_s Z_s) / [1 - (X_s / Z_s) Z_0 X_0]$, where X_s and X_0 are defined as $X_s = \tan(\beta_s l_1)$ and $X_0 = \tan(\beta_0 l_2)$. The reflection coefficient Γ is given by: $\Gamma = (Z_1 - Z_0) / (Z_1 + Z_0)$. The reflected power is proportional to $|\Gamma|^2$. These equations were used to calculate the reflected power using different dielectrics and compare them with experimental results.

III. EXPERIMENTAL RESULTS

A. Array of Local Scatterers and Imaging at 10 GHZ

As can be seen from fig. 3, the face of the motor is metallic and is semi-cylindrical and reflects the incident polarized microwave with varying intensity thus modulating it at the frequency of motor excitation. Fig. 4 shows the received spectrums for the reflected signals for no sample and $\epsilon_r = 2.2$ sample, which clearly demonstrates the detecting capability of the system.

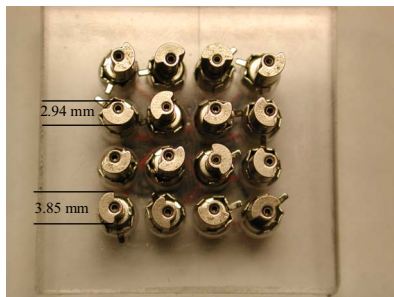


Figure 3. Motor Array.

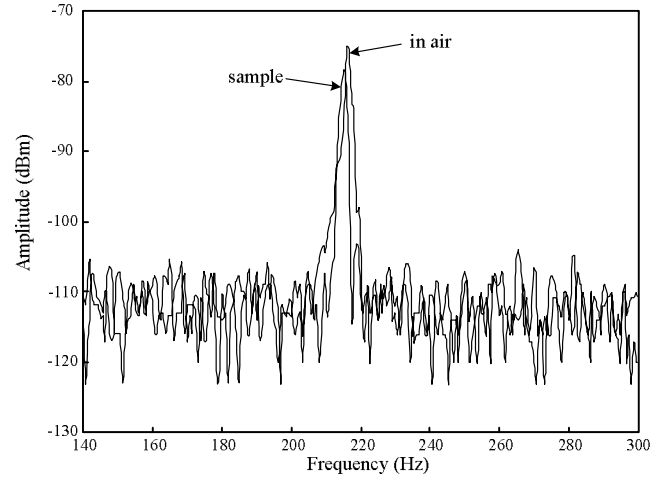


Figure 4. The change of received spectrum when a sample of $\epsilon_r = 2.2$ was placed between the motor array and the horn antenna.

Fig. 5 shows the calibration results and the calculated values using the equations discussed above at 500 μm distance from the horn antenna to the sample. The calculated values using the simple model are in good agreement with the experimental data. Larger working distances can be achieved with higher sensitivity receiver. The samples are RT Duroids with the known permittivities. The thickness of each sample was around 640 μm .

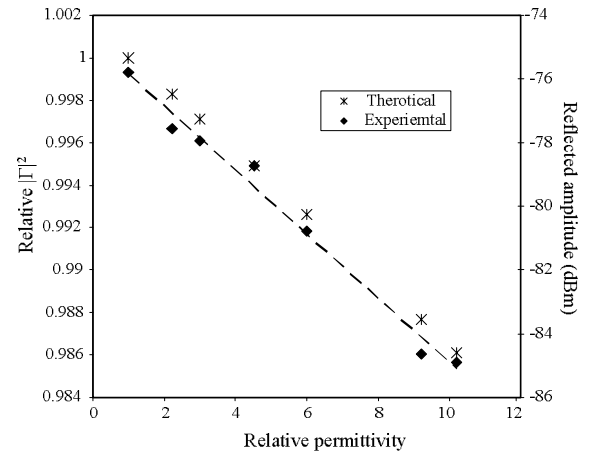


Figure 5. Calibration curve with simulation values.

The above measurements were repeated ten times for reproducibility test, which showed the variation of each measurement to be as small as 1%. In addition to short term reproducibility test, we also investigated the long term stability of the system. The variation was around 2% for a 30 minute measurement.

Because it is a non-destructive technique, it generally requires very little specimen preparation as long as the size of the specimen is smaller than the total working area of horn antenna. Fig. 6 shows a dielectric map image around 2.3 cm

in both directions. The image shows a sample with 16 different permittivity regions scanned with the corresponding 16 motors. The permittivity was labeled on each corresponding section. The image not only shows the ability of the probe to scan large single layer sample, but also reveals the ability of the system to detect change in multiple-layered structure.

It should be noted that errors in calibration will result in erroneous dielectric constant measurements. Therefore, calibration must be checked prior to each measurement cycle.

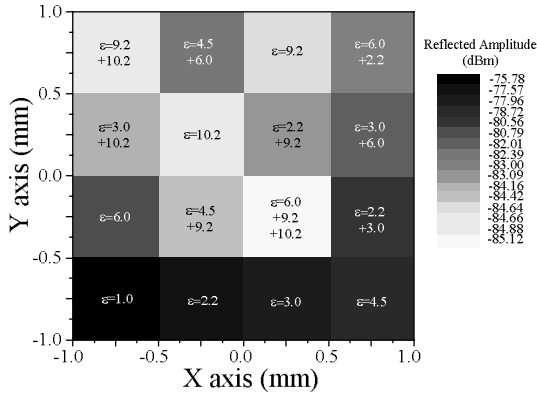


Figure 6. Image for different kinds of samples.

B. Array of Local Scatterers and Imaging at 100 GHz

As shown in fig. 7, the AFM operation is based upon using an optical detection method to track vertical (z) motion of the cantilever beam tip that is scanned over a sample. An optical detection method is used to detect deflections of the cantilever beam caused by tip-sample interactions. The AFM probe follows the sample's topography and an image is constructed by monitoring tip displacement across the sample. Many different AFM imaging modes are developed, including noncontact, contact, tapping, and shear-force imaging. The addition of a microwave signal to the probe tip enables simultaneous AFM and microwave imaging of the sample. The microwave signal can be viewed as an illumination of the sample's interior, enabling imaging embedded structures and nonuniformity in the microwave property of the sample. The coupling section of the AFM tip and the sample is modeled as shown in fig. 7. Since the tip section is much smaller than the wavelength in our experiment ($f = 100$ GHz with $\lambda_{free} = 3$ mm), we can simply model it as a capacitor (C_p). The tip-sample interaction is modeled by the coupling capacitance C_c in the noncontact mode. Semiconductor and insulating samples are modeled by a resistance (R_s) and a capacitance (C_s), as shown in fig. 7.

The experimental setup used for the scanning near-field microwave microscopy is shown in fig. 8. The measurement were performed using a 100 GHz mechanically tuned Gunn diode oscillator. Directional coupler circulated the signal from the oscillator to the sample under test, and directed the reflected wave from the AFM tip to a waveguide detector.

The output signal from the detector was then fed to the AFM imaging system and images were generated in real time.

The images shown in fig. 9 were simultaneously obtained with the scanning near-field microwave microscopy/AFM system in our group. They show the images of carbon nanotubes on the titanium film substrate. As can be seen clearly, the patterns obtained from the near-field microwave microscopy are comparable to those from AFM system. The above two images illustrate bundles of carbon nanotubes with additional graphitic carbon on them (1-5 μ m). The below two images exhibit multi-walled carbon nanotubes with around 100 nm diameter.

To reduce AFM-based modulated scatterers system scanning time, an array of conducting probes can be microfabricated as schematically shown in fig. 10. Each probe in the array can be excited electrostatically at different frequencies. This approach is scalable and cost effective. However, it requires that each array member to be dynamically adjustable to regulate their stand-off distances with samples with large topographical variations.

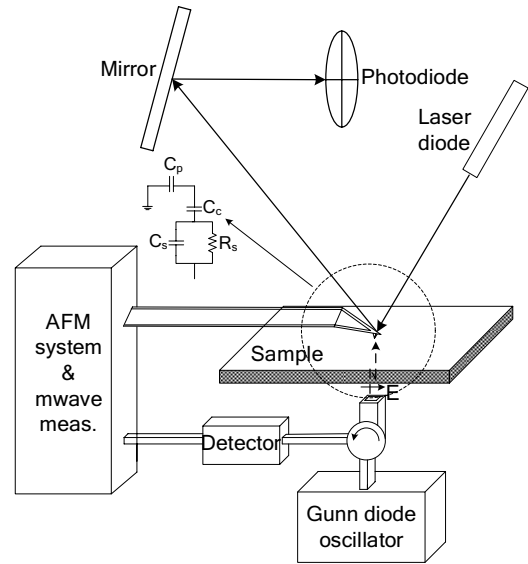


Figure 7. Schematic of near-field microwave measurement with a commercial AFM system.

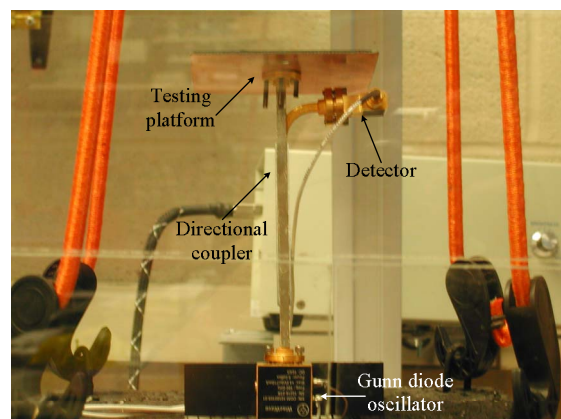


Figure 8. Scanning near-field microwave microscopy experimental setup with AFM system.

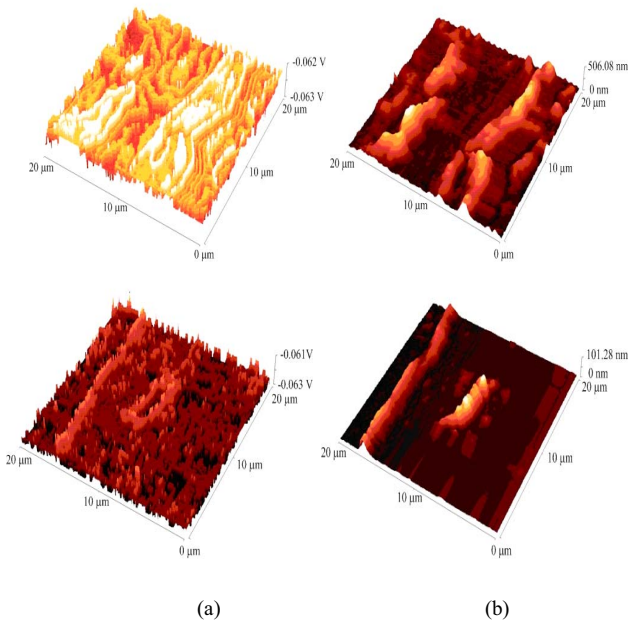


Figure 9. Simultaneous images obtained from (a) the near-field microwave microscope, and (b) the AFM system. The scan was performed at 100 GHz through a thin layer of titanium with carbon nanotubes on it.

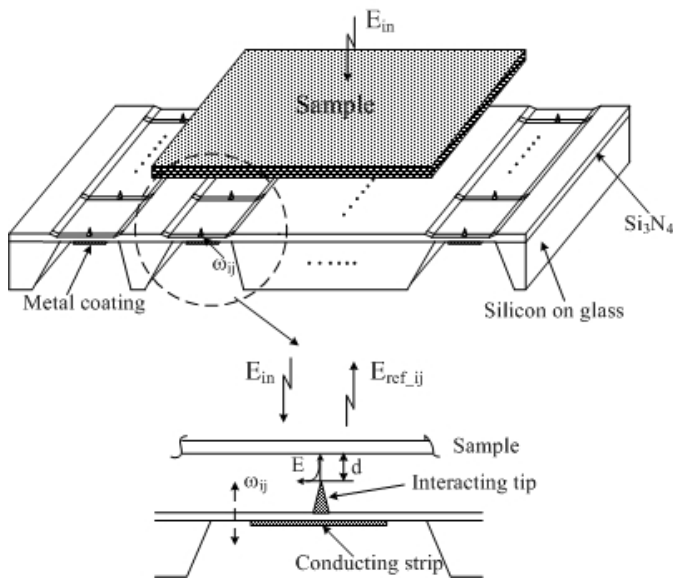


Figure 10. A MEMS array of local scatterers.

IV. DISCUSSION AND CONCLUSION

In this research, near-field microwave imaging system integrated with AFM were implemented and used to image materials properties with high resolutions. We also proposed and implemented the unique technique using modulated scatterers combining the aspects of “free-space” imaging with near-field microwave resolution. We discussed the application of this technique by imaging dielectric sample at 10 GHz using

an array of micromotors as scatterers, and carbon nanotubes at 100 GHz using an atomic force microscope tip as the local scatterer.

REFERENCES

- [1] G. Binnig, H. Rohrer, C. Gerber, and E. Weibel, “7x7 reconstruction on Si (111) resolved in real space,” *Phys. Rev. Lett.*, vol. 50, pp. 120–123, 1983.
- [2] A. Kleiner and S. Eggert, “Curvature, hybridization, and STM images of carbon nanotubes,” *Phys. Rev. B, Condens. Matter*, vol. 64, no. 113 402, pp. 1–4, 2001.
- [3] N. Nilius, N. Ernst, and H.-J. Freund, “Tip influence on plasmon excitations in single gold particles in an STM,” *Phys. Rev. B, Condens. Matter*, vol. 65, no. 115 421, pp. 1–8, 2001.
- [4] J. Nieminen, S. Lahti, S. Paavilainen, and K. Morgenstern, “Contrast changes in STM images and relations between different tunneling models,” *Phys. Rev. B, Condens. Matter*, vol. 66, no. 165 421, pp. 1–9, 2002.
- [5] S. Urazhdin, S. H. Tessler, and R. C. Ashoori, “A simple low-dissipation amplifier for cryogenic STM,” *Rev. Sci. Instrum.*, vol. 73, pp. 310–312, 2002.
- [6] M. Tabib-Azar, and D. Akinwande, “Real-time imaging of semiconductor space-charge regions using high-spatial resolution evanescent microwave microscope” *Rev. Sci. Instrum.*, vol. 71, pp. 1460-1465, 2000.
- [7] M. Tabib-Azar, D. Akinwande, G. Ponchak, and S. R. LeClair, “Novel physical sensors using evanescent microwave probes,” *Rev. Sci. Instrum.*, vol. 70, pp. 3381-3386, 1999.
- [8] M. Tabib-Azar, D. Akinwande, G. Ponchak, and S. R. LeClair, “Evanescent microwave probes on high-resistivity silicon and its application in characterization of semiconductors,” *Rev. Sci. Instrum.*, vol. 70, pp. 3083-3086, 1999.
- [9] M. Tabib-Azar, R. Ciocan, G. Ponchak, and S. R. LeClair, “Transient thermography using evanescent microwave microscope,” *Rev. Sci. Instrum.*, vol. 70, pp. 3387-3390, 1999.
- [10] M. Tabib-Azar, and B. Sutapun, “Novel hydrogen sensors using evanescent microwave probes,” *Rev. Sci. Instrum.*, vol. 70, pp. 3707-3713, 1999.
- [11] M. Tabib-Azar, N. Shoemaker, and S. Harris, “Non-destructive Characterization of Materials by Evanescent Microwaves,” *Measurement Science and Technology*, pp. 583-590, 1993.
- [12] M. Tabib-Azar, D. P. Su, S. LeClair, and G. Pochak, “0.4 μm spatial resolution with 1 GHz ($\lambda = 30$ cm) evanescent microwave probe,” *Review of Scientific Instruments*, vol. 70, pp. 1725-1729, 1999.
- [13] W. M. Duncan, “Near-field scanning optical microscope for microelectronic materials and devices,” *J. Vac. Sci. Technol. A, Vac. Surf. Films*, vol. 14, pp. 1914–1918, 1996.
- [14] M. Tabib-Azar, and Y. Wang, “Design and fabrication of scanning near-field microwave probes compatible with atomic force microscopy to imaging embedded nanostructures,” *IEEE Trans. Microwave Theory and Tech.*, vol. 52, pp. 971-979, 2004.
- [15] Y. Wang, and M. Tabib-Azar, “Microfabricated near-field microwave probes for scanning microscopy,” *12th Intl. Conf. Transducers, Solid-State Sensors, Actuators and Microsystems*, 2003.
- [16] M. Tabib-Azar, and J. L. Katz, “Evanescent microwaves: a novel super-resolution noncontact nondestructive imaging technique for biological applications,” *IEEE Trans. on Instrument and Measurement*, vol. 48, pp. 1111-1116, 1999.
- [17] P. Grütter, D. Rugar, H. J. Mamin, G. Castillo, S. E. Lambert, C.-J. Lin, R. M. Valletta, O. Wolter, T. Bayer, and J. Greschner, “Batch fabrication sensors for magnetic force microscopy,” *Appl. Phys. Lett.*, vol. 57, pp. 1820–1822, 1990.
- [18] A. DiCarlo, M. R. Scheinfein, and R. V. Chamberlin, “Magnetic force microscopy utilizing an ultrasensitive vertical cantilever geometry,” *Appl. Phys. Lett.*, vol. 61, pp. 2108–2110, 1992.
- [19] G. D. Skidmore and E. D. Dahlberg, “Improved spatial resolution in magnetic force microscopy,” *Appl. Phys. Lett.*, vol. 71, pp. 3293–3295, 1997.

- [20] T. G. Sorop, C. Untiedt, F. Luis, M. Kröll, M. Rasa, and L. J. de Jongh, "Magnetization reversal of ferromagnetic nanowires studied by magnetic force microscopy," *Phys. Rev. B, Condens. Matter*, vol. 67, no. 014 402, pp. 1–8, 2003.
- [21] R. Zoughi, and S. Bakhtiari, "Microwave nondestructive detection and evaluation of disbanding and delamination in layered-dielectric-slabs," *IEEE Transactions on Instrumentation and Measurement*, vol. 39, pp. 1059-1063, Dec, 1990.
- [22] R. Zoughi, and M. Lujan, "Nondestructive microwave thickness measurement of dielectric slabs," *Materials Evaluation*, vol. 48, pp. 1100-1105, Sep, 1990.
- [23] C. Gabriel, S. Gabriel, and E. Corthout, "The dielectric properties of biological tissues: I. Literature survey," *Phys. Med. Biol.*, vol. 41, pp. 2231-2249, 1996.
- [24] S. Gabriel, R. W. Lau, and C. Gabriel, "The dielectric properties of biological tissues: II. Measurement on the frequency range 10 Hz to 20 GHz," *Phys. Med. Biol.*, vol. 41, pp. 2251-2269, 1996.
- [25] K. R. Foster, and H. P. Schwan, "Dielectric properties of tissues and biological materials: A critical review," *Crit. Rev. Biomed. Eng.*, vol. 17, pp. 25-104, 1989.
- [26] P. M. Meaney, K. D. Paulsen, B. W. Pogue, and M. I. Miga, "Microwave image reconstruction utilizing log-magnitude and unwrapped phase to improve high-contrast object recovery," *Transactions on Medical Imaging*, vol. 20, pp. 104-116, Feb, 2001.
- [27] W. C. Chew, "Imaging and inverse problems in electromagnetics," in *Advances in computational Electrodynamics*, A. Taflove, Ed. Norwood, Ma, Artech, 1988.
- [28] S. Y. Semenov, R. H. Bulyshev, and etc, "Three-dimensional microwave tomography: initial experimental imaging of animals," *Transactions on Biomedical Engineering*, vol. 49, pp. 55-63, 2002.
- [29] E. C. Fear, S. C. Hagness and etc, "Enhancing breast tumor detection with near-field imaging," *IEEE Microwave Magazine*, vol. 3, pp. 48-56, Mar, 2002.